Inorg. Chem. **2007**, *46*, 2596–2603

Synthesis, Structure, and Properties of Low-Spin Manganese(III)–Poly(pyrazolyl)borate Complexes

Ferdaus Hossain,[†] Matthew A. Rigsby,[†] Cole T. Duncan,[†] Paul L. Milligan, Jr.,[†] Richard L. Lord,[‡] Mu-Hyun Baik,*[,‡] and Franklin A. Schultz*[,†]

Department of Chemistry and Chemical Biology, Indiana University–Purdue University Indianapolis, 402 North Blackford Street, Indianapolis, Indiana 46202, and Department of Chemistry and School of Informatics, Indiana University, Bloomington, Indiana 47405

Received November 22, 2006

The manganese(III)-bis[poly(pyrazolyl)borate] complexes, $Mn(pzb)_2SbF_6$, where pzb^- = tetrakis(pyrazolyl)borate (pzTp) (**1**), hydrotris(pyrazolyl)borate (Tp) (**2**), or hydrotris(3,5-dimethylpyrazolyl)borate (Tp*) (**3**), have been synthesized by oxidation of the corresponding $Mn(pzb)_2$ compounds with $NOSbF_6$. The Mn(III) complexes are low-spin in solution and the solid state (μ_{eff} = 2.9–3.8 μ_B). X-ray crystallography confirms their uncommon low-spin character. The close conformity of mean Mn–N distances of 1.974(4), 1.984(5), and 1.996(4) Å in **1**, **2**, and **3**, respectively, indicates absence of the characteristic Jahn–Teller distortion of a high-spin d^4 center. N–Mn–N bite angles of slightly less than 90° within the facially coordinated pzb^- ligands produce a small trigonal distortion and effective D_{3d} symmetry in **1** and **2**. These angles increase to 90.0(4)° in **3**, yielding an almost perfectly octahedral disposition of N donors in $Mn(Tp^*)_2^+$. Examination of structural data from 23 metal–bis(pzb) complexes reveals systematic changes within the metal–(pyrazolyl)borate framework as the ligand is changed from pzTp to Tp to Tp*. These deformations consist of significant increases in M–N–N, N–B–N, and N–N–B angles and a minimal increase in Mn–N distance as a consequence of the steric demands of the 3-methyl groups. Less effective overlap of pyrazole lone pairs with metal atom orbitals resulting from the M–N–N angular displacement is suggested to contribute to the lower ligand field strength of Tp* complexes. $Mn(pzb)_2^+$ complexes undergo electrochemical reduction and oxidation in CH_3CN. The electrochemical rate constant ($k_{s,h}$) for reduction of t_{2g}^4 $Mn(pzb)_2^+$ to $t_{2g}^3e_g^2$ $Mn(pzb)_2$ (a coupled electron-transfer and spin-crossover reaction) is 1–2 orders of magnitude smaller than that for oxidation of t_{2g}^4 $Mn(pzb)_2^+$ to t_{2g}^3 $Mn(pzb)_2^{2+}$. $k_{s,h}$ values decrease as Tp* > pzTp > Tp for the $Mn(pzb)_2^{+/0}$ electrode reactions, which contrasts with the behavior of the comparable $Fe(pzb)_2^{+/0}$ and $Co(pzb)_2^{+/0}$ couples.

Introduction

Manganese is an important and widespread element.[1] Its occurrence in a number of redox enzymes (e.g., catalase, peroxidase, superoxide dismutase),[2,3] in the oxygen-evolving center (OEC) of photosystem II,[4–6] and in single-molecule magnets[7] has stimulated interest in its properties and reactivities, especially in oxidation states II, III, and IV. Many investigations have employed the versatile poly(pyrazolyl)-borate (pzb^- = pzTp, Tp, or Tp*) ligands,[8,9] and homoleptic

* To whom correspondence should be addressed. E-mail: schultz@chem.iupui.edu (F.A.S.); mbaik@indiana.edu (M.-H.B.).
† Indiana University–Purdue University Indianapolis.
‡ Indiana University.

(1) (a) Cotton, F.A.; Wilkinson, G.; Murillo, C.A.; Bochmann, M. *Advanced Inorganic Chemistry*, 6th ed.; John Wiley and Sons: New York, 1999; pp 757–775. (b) Weatherburn, D.C.; Mandel, S.; Mukopadhyay, S.; Bhaduri, S.; Lindoy, L.F. In *Comprehensive Coordination Chemistry II*, 2nd ed.; McCleverty, J.A., Meyer, T.J., Eds.; Elsevier: Amsterdam, 2004; Vol. 5, Chapter 5.1. (c) Schultz, F. A.; Duncan, C. T.; Rigsby, M. A. In *Encyclopedia of Electrochemistry*; Bard, A. J., Stratmann, M., Eds.; Scholz, F., Pickett, C. J., Eds.; Wiley-VCH: Weinheim, 2006; Vol. 7a: Inorganic Electrochemistry, pp 399–460.
(2) *Manganese Redox Enzymes*; Pecoraro, V. L., Ed.; VCH Publishers: New York, 1992.
(3) *Metal Ions in Biological Systems*; Sigel, A., Sigel, H., Eds.; Marcel Dekker: Basel, 2000; Vol. 37.
(4) Yachandra, V. K.; Sauer, K.; Klein, M. P. *Chem. Rev.* **1996**, *96*, 2927–2950.
(5) Tommos, C.; Babcock, G. T. *Acc. Chem. Res.* **1998**, *31*, 18–25.
(6) Mukhopadhyay, S.; Mandal, S. K.; Bhaduri, S.; Armstrong, W. H. *Chem. Rev.* **2004**, *104*, 3981–4026.
(7) Soler, M.; Wernsdorfer, W.; Abboud, K. A.; Huffman, J. C.; Davidson, E. R.; Hendrickson, D. N.; Christou, G. *J. Am. Chem. Soc.* **2003**, *125*, 3576–3588.
(8) Trofimenko, S. *Scorpionates—The Coordination Chemistry of Polypyrazolylborate Ligands*; Imperial College Press: London, 1999.

10.1021/ic062224+ CCC: $37.00
Published on Web 03/02/2007

Scheme 1

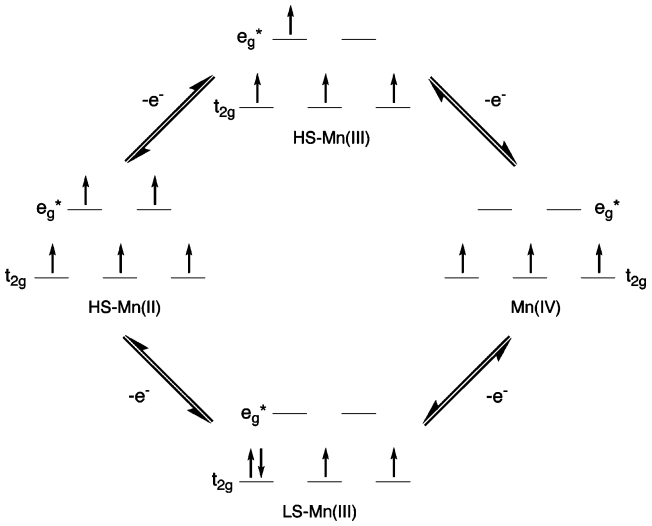

bis(pzb) complexes of Mn(II) [$Mn(pzTp)_2$,[10] $Mn(Tp)_2$,[10] and $Mn(Tp^*)_2$[11]] and Mn(IV) {$[Mn(Tp^*)_2](ClO_4)_2$}[12] have been isolated and structurally characterized. Heretofore, the corresponding Mn(III) complexes have not been studied in this manner.

Our interest in these compounds derives from the position of Mn(III) between the $t_{2g}^3e_g^2$ Mn(II) and t_{2g}^3 Mn(IV) oxidation states, which leads to the question illustrated in Scheme 1: Does stepwise Mn(II) → Mn(III) → Mn(IV) electron transfer proceed through high-spin ($t_{2g}^3e_g^1$) or low-spin (t_{2g}^4) Mn(III)? The answer is central to understanding the redox behavior of Mn in many of its biological applications and in understanding the thermodynamics and kinetics of electron-transfer reactions that are coupled to spin crossover.[13] Recently, we surveyed the electrochemical, magnetic, and spectroscopic properties of a number of metal−bis(pzb) complexes[14] and reported the Mn(III) examples to be low-spin on the basis on their room-temperature magnetic moments. This result was not anticipated because mononuclear low-spin Mn(III) is uncommon. Rare examples include the hexacyanomanganate(III) ion[15] and complexes with tetradentate macrocyclic equatorial and unidentate strong-field axial ligands.[16] Among complexes which contain a $Mn^{III}N_6$ coordination environment, $[Mn(sar)](NO_3)_3{\cdot}H_2O$[17] is high-spin at room temperature, whereas Mn(taa)[18] is a true spin-crossover complex that exhibits an abrupt $S = 1$ to $S = 2$ transition at 40−50 K. Recently, Wieghardt et al.[19] reported a $S = 0$ $Mn^{III}(L^{\bullet-})_2^+$ complex in which the two unpaired electrons of low-spin Mn(III) are antiferromagnetically coupled to the unpaired electrons of the monoanionic radical pyridine-2,6-diimine ligands ($L^{\bullet-}$), and Morgan et al.[20] reported a Mn(III) complex of a hexadentate N_4O_2 Schiff base ligand with trans phenolate donors, which undergoes low-to-high-spin crossover at 100−300 K.

On the basis of these observations, we decided to explore the nature of the $Mn(pzb)_2^+$ complexes more completely and report here the synthesis and X-ray structural characterization of $[Mn(pzTp)_2]SbF_6$, $[Mn(Tp)_2]SbF_6$, and $[Mn(Tp^*)_2]SbF_6$ and additional studies of their electrochemical, magnetic, and spectroscopic properties.

Experimental Section

Materials. The following reagents were obtained from commercial sources and used as received: $MnCl_2{\cdot}4H_2O$ (Alfa Aesar), KpzTp (Acros), and KTp and KTp* (Strem).

Syntheses. $Mn(pzb)_2$ complexes were prepared by mixing aqueous solutions of $MnCl_2{\cdot}4H_2O$ and the potassium salt of the ligand in stoichiometric proportions.[21] The white $Mn(pzb)_2$ solids were collected and recrystallized from 1,2-dichloroethane or acetonitrile.

$[Mn(pzTp)_2]SbF_6$ (1). To 0.382 g (0.62 mmol) of $Mn(pzTp)_2$ in 300 mL of 1:1 CH_3CN/CH_2Cl_2 was added 0.172 g (0.65 mmol) of $NOSbF_6$. The solution turned pale yellow while being stirred for a period of 2 h. The solution was filtered and evaporated to yield a finely powdered yellow solid, which was recrystallized from CH_3CN. Yield: 0.529 g, 98%. μ_{eff} (solid): 3.26 μ_B. UV/vis in CH_3CN. λ_{max}, nm (log ϵ, M^{-1} cm^{-1}): 270 (4.11), 345 (3.93), 388 (sh) (3.76). Anal. Calcd for $C_{24}H_{24}N_{16}B_2MnSbF_6$: C, 33.96; H, 2.85; N, 26.40; Mn, 6.47. Found: C, 33.87; H, 3.11; N, 26.14; Mn, 6.11.

$[Mn(Tp)_2]SbF_6$ (2). To 1.286 g (2.67 mmol) of $Mn(Tp)_2$ in CH_3CN was added 0.742 g (2.78 mmol) of $NOSbF_6$. The solution turned yellow and was stirred for 30 min. A yellow solid, obtained upon filtration and evaporation of the solvent, was recrystallized twice from CH_3CN. Yield: 1.72 g, 90%. μ_{eff} (solid): 2.95 μ_B. UV/vis in CH_3CN. λ_{max}, nm (log ϵ, M^{-1} cm^{-1}): 267 (3.92), 342 (3.97), 385 (sh) (3.54). Anal. Calcd for $C_{18}H_{20}N_{12}B_2MnSbF_6$: C, 30.16; H, 2.81; N, 23.45; Mn, 7.66. Found: C, 30.08; H, 3.00; N, 23.38; Mn, 7.48.

(9) Abbreviations: pzTp = tetrakis(pyrazol-1-yl)borate; Tp = hydrotris(pyrazol-1-yl)borate; Tp* = hydrotris(3,5-dimethylpyrazol-1-yl)borate; Tp^{Me} = hydrotris(3-methylpyrazol-1-yl)borate; *t*-BuTp = *tert*-butyltris(pyrazol-1-yl)borate; *t*-$BuTp^{Me}$ = *tert*-butyltris(3-methylpyrazol-1-yl)borate; taa^{3-} = trianion of tris(1-(2-azolyl)-2-azabuten-4-yl)amine; sar = 3,6,10,13,16,19-hexaazabicyclo[6.6.6]icosane (sarcophagine); $acac^-$ = acetylacetonate; $trop^-$ = anion of 2-hydroxy-2,4,6-cycloheptatrienone (tropolone); $TBAPF_6$ = tetra-*n*-butylammonium hexfluorophosphate; $tripod^-$ = cyclopentadienyl-tris(diethylphosphito-P)-cobaltate(1−).

(10) Kitano, T.; Sohrin, Y.; Hata, Y.; Kawakami, H.; Hori, T.; Ueda, K. *J. Chem. Soc., Dalton Trans.* **2001**, 3564−3571.
(11) Xing, Y. H.; Aoki, K.; Bai, F. Y. *Synth. React. Inorg. Metal-Org. Chem.* **2004**, *34*, 1149−1163.
(12) Chan, M. K., Armstrong, W. H. *Inorg. Chem.* **1989**, *28*, 3777−3779.
(13) (a) Turner, J. W.; Schultz, F.A.; *Coord. Chem. Rev.* **2001**, *219−221.*, 81−97; (b) Turner, J. W.; Schultz, F. A. *J. Phys. Chem. B* **2002**, *106*, 2009−2017.
(14) De Alwis, C. D. L.; Schultz, F. A. *Inorg. Chem.* **2003**, *42*, 3616−3622.
(15) (a) Alexander, J. J.; Gray, H. B. *J. Am. Chem. Soc.* **1968**, *90*, 4260−4271. (b) Chawla, I. D.; Frank, M. J. *J. Inorg. Nucl. Chem.* **1970**, *32*, 555−563. (c) Buschmann, W. E.; Liable-Sands, L.; Rheingold, A. L.; Miller, J. S. *Inorg. Chim. Acta* **1999**, *284*, 175−179.
(16) (a) Hansen, A. P.; Goff, H. M. *Inorg. Chem.* **1984**, *23*, 4519−4525. (b) Galich, L.; Hückstädt, H.; Homborg, H. *J. Porphyrins Phthalocyanines* **1998**, *2*, 79−87. (c) Mossin, S.; Sørensen, H. O.; Weihe, H. *Acta Crystallogr.* **2002**, *C58*, m204−m206. (d) Matsuda, M.; Yamaura, J.-I.; Tajima, H.; Inabe, T. *Chem. Lett.* **2005**, *34*, 1524−1525.
(17) Anderson, P. A.; Creaser, I. I.; Dean, C.; Harrowfield, J. M.; Horn, E.; Martin, L. L.; Sargeson, A. M.; Snow, M. R.; Tiekink, E. R.T. *Aust. J. Chem.* **1993**, *46*, 449−463.
(18) (a) Sim, P. G.; Sinn, E. *J. Am. Chem. Soc.* **1981**, *103*, 241−243. (b) Nakano, M.; Matsubayashi, G.; Matsuo, T. *Phys. Rev. B* **2002**, *66*, 212412. (c) Kimura, S.; Narumi, Y.; Kindo, K.; Nakano, M.; Matsubayashi, G. *Phys. Rev. B* **2005**, *72*, 064448. (d) Guionneau, P.; Marchivie, M.; Garcia, Y.; Howard, J. A. K.; Chasseau, D. *Phys. Rev. B* **2005**, *72*, 214408.
(19) de Bruin, B.; Bill, E.; Bothe, E.; Weyhermüller, T.; Wieghardt, K. *Inorg. Chem.* **2000**, *39*, 2936−2947.
(20) Morgan, G. G.; Murnaghan, K. D.; Müller-Bunz, H.; McKee, V.; Harding, C. J. *Angew. Chem., Int. Ed.* **2006**, *45*, 7192−7195.
(21) Trofimenko, S. *Inorg. Synth.* **1970**, *12*, 99−109.

Table 1. Crystallographic Data for $[Mn(pzTp)_2]SbF_6$ (**1**), $[Mn(Tp)_2]SbF_6$ (**2**), and $[Mn(Tp^*)_2]SbF_6$ (**3**)[a]

	1	**2**	**3**
empirical formula	$C_{24}H_{24}B_2F_6MnN_{16}Sb$	$C_{18}H_{20}B_2F_6MnN_{12}Sb$	$C_{30}H_{44}B_2F_6MnN_{12}Sb$
fw	848.90	716.77	885.08
temp	130(2) K	120(2) K	120(2) K
cryst syst, space group	monoclinic, *C*2/*c*	triclinic, $P\bar{1}$	monoclinic, $P2_1/c$
unit cell dimens	$a = 17.4593(16)$ Å	$a = 7.5518(2)$ Å	$a = 10.4142(4)$ Å
	$\alpha = 90^o$	$\alpha = 99.097(1)^o$	$\alpha = 90^o$
	$b = 20.0737(18)$ Å	$b = 8.8710(2)$ Å	$b = 14.1854(6)$ Å
	$\beta = 118.728(2)^o$	$\beta = 91.782(1)^o$	$\beta = 94.2700(10)^o$
	$c = 10.2596(9)$ Å	$c = 9.9838(3)$ Å	$c = 12.4063(5)$ Å
	$\gamma = 90^o$	$\gamma = 108.516(1)^o$	$\gamma = 90^o$
vol	3153.1(5) Å^3	623.87(3) Å^3	1827.69(3) Å^3
Z	4	1	2
calcd density	1.788 Mg m^{-3}	1.908 Mg m^{-3}	1.608 Mg m^{-3}
abs coeff	1.340 mm^{-1}	1.670 mm^{-1}	1.157 mm^{-1}
final *R* indices [$I > 2\sigma(I)$]	R1 = 0.0350	R1 = 0.0210	R1 = 0.0334
	wR2 = 0.0823	wR2 = 0.0546	wR2 = 0.0923
R indices (all data)	R1 = 0.0426	R1 = 0.0230	R1 = 0.0476
	wR2 = 0.0878	wR2 = 0.0562	wR2 = 0.1017

[a] GOF = $[\sum[w(F_o^2 - F_c^2)^2]/(N_{observations} - N_{parameters})]^{1/2}$, all data. R1 = $\sum(|F_o| - |F_c|)/\sum|F_o|$. wR2 = $[\sum[w(F_o^2 - F_c^2)^2]/\sum[w(F_o^2)^2]]^{1/2}$.

$[Mn(Tp^*)_2]SbF_6$ (3). To 0.123 g (0.19 mmol) of $Mn(Tp^*)_2$ in 50 mL of 1,2-dichloroethane was added 0.052 g (0.20 mmol) of $NOSbF_6$. The solution turned pale yellow while being stirred for a period of 2 h. The solution was filtered and evaporated, and the resulting yellow solid was recrystallized from warm acetonitrile. Yield: 0.109 g, 65%. μ_{eff} (solid): 3.83 μ_B. UV/vis in CH_3CN. λ_{max}, nm (log ϵ, M^{-1} cm^{-1}): 277 (3.80), 364 (3.94), 420 (sh) (3.38). Anal. Calcd for $C_{30}H_{44}N_{12}B_2MnSbF_6$: C, 40.71; H, 5.01; N, 19.00; Mn, 6.21. Found: C, 40.61; H, 5.20; N, 19.12; Mn, 5.77.

X-ray Structure Determinations. Crystals suitable for X-ray analysis, which were obtained by vapor diffusion of hexane into acetonitrile solutions of **1**, **2**, and **3**, were mounted on the tip of a glass capillary in a SMART6000 CCD diffractometer (Bruker). Data collection was carried out by use of Mo Kα radiation (graphite monochromator, $\lambda = 0.71073$ Å). Final cell constants were calculated from the *xyz* centroids of 4492, 6983, and 2816 strong reflections from the actual data collection for **1**, **2**, and **3**, respectively, after integration (SAINT).[22] The intensity data were corrected for absorption (SADABS).[23] The space groups were determined by intensity statistics and systematic absences. Structures were solved using SIR-92[24] and refined with SHELXL-97.[25] A direct-methods solution was calculated, which provided most non-hydrogen atoms from the E-map. Full-matrix least-squares/difference Fourier cycles were performed, which located the remaining non-hydrogen atoms. All non-hydrogen atoms were refined with anisotropic displacement parameters. The hydrogen atoms were placed in ideal positions and refined as riding atoms with individual isotropic displacement parameters. In **2** and **3**, the Mn and Sb atoms are located in special positions, and the Mn complex and the counterion have inversion symmetry. In **1**, nonclassical hydrogen bonding[26] is observed between the Mn complex and the counterion: C3−H3···F2, 2.370 Å, 168.3°, and C7−H7···F3, 2.468 Å, 133.4°. Further crystallographic data and refinement information are presented in Table 1.

Physical Measurements. Electronic spectra were recorded by use of an HP 8453A spectrometer. Magnetic moments of solids were determined with a Johnson Matthey MSB-1 susceptibility balance. Magnetic moments in solution were determined as a function of temperature as described previously by use of the ^{1}H NMR method of Evans.[27] These measurements were conducted in CH_3CN-d_3 for **1** and **2** and in DMF-d_7 for **3**. Elemental analyses were performed by Huffman Laboratories, Golden, CO.

Electrochemical measurements were conducted in a three-electrode cell consisting of a glassy carbon working electrode (Bioanalytical Systems, MF-2012, area = 0.071 cm^2), a Pt auxiliary electrode, and a Ag/AgCl (3 M NaCl) reference electrode (Bioanalytical Systems, MF-2079). The working electrode was polished with an aqueous suspension of 0.05-μm alumina (Buehler), rinsed with deionized water, and rinsed with solvent before use. Potentials are reported versus that of the ferrocene/ferricenium ($Fc^{+/0}$) couple, which was determined to be +0.44(1) V vs Ag/AgCl under the experimental conditions.

Cyclic voltammetry (CV) experiments were conducted at 298 K in acetonitrile (Burdick and Jackson, distilled-in-glass reagent) containing 0.1 M $TBAPF_6$ as supporting electrolyte. Data were collected by use of an EG&G PAR 273A potentiostat. Values of the standard heterogeneous electron-transfer rate constant, $k_{s,h}$, were determined from the peak potential separation, ΔE_p, of background-subtracted voltammograms at scan rates of $\upsilon = 0.025-0.25$ V s^{-1}. Approximately 90% of the estimated solution resistance (calculated as $R = \rho/4r$, where $\rho = 109$ Ω cm is the resisitivity of 0.1 M $TBAPF_6/CH_3CN$[28] and r is the electrode radius) was compensated electronically. $k_{s,h}$ was determined from the published relationship[29a] between ΔE_p and the kinetic parameter, ψ, for $\Delta E_p < 250$ mV and from eq 1 in ref 29b for $\Delta E_p > 250$ mV. Values of $\alpha = \beta = 0.50$ and a diffusion coefficient, *D*, determined from the linear relationship between voltammetric peak current, i_p, and $\upsilon^{1/2}$ were used in these calculations.

Results and Discussion

Synthesis and Characterization. Manganese(III) complexes **1**−**3** were prepared in high yield in a straightforward

(22) *SAINT Current Version*; Bruker Analytical X-ray Systems: Madison, WI.
(23) Blessing, R. H. *Acta Crystallogr.* **1995**, *A51*, 33−38.
(24) Altomare, A.; Cascarno, G.; Giacovazzo, C.; Gualardi, A. *J. Appl. Cryst.* **1993**, *26*, 343−350.
(25) *SHELXL-Plus Current Version*; Bruker Analytical X-ray Systems: Madison, WI.
(26) Taylor, R.; Kennard, O. *J. Am. Chem. Soc.* **1982**, *104*, 5063−5070.
(27) (a) Turner, J. W.; Schultz, F. A. *Inorg. Chem.* **2001**, *40*, 5296−5298; (b) Evans, D.F. *J. Chem. Soc.* **1959**, 2003−2005.
(28) Bowyer, W. J.; Engelman, E. E.; Evans, D. H. *J. Electroanal. Chem.* **1989**, *262*, 67−82.
(29) (a) Bard, A.J.; Faulkner, L.R. *Electrochemical Methods: Fundamentals and Applications*, 2nd ed.; Wiley: New York, 2001, Chapter 6. (b) Schultz, F. A. *J. Electroanal. Chem.* **1986**, *213*, 169−174.

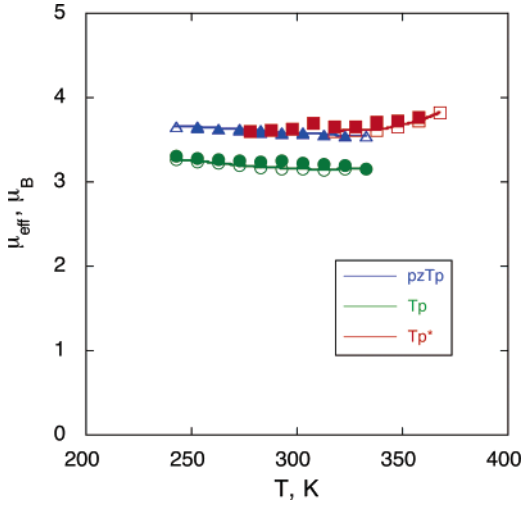

Figure 1. Magnetic moments of $Mn(pzb)_2^+$ complexes in CH_3CN-d_3 (pzTp, Tp) and DMF-d_7 (Tp*) as a function of temperature. Open and filled symbols represent warming and cooling cycles, respectively. Lines are drawn as a guide to the eye.

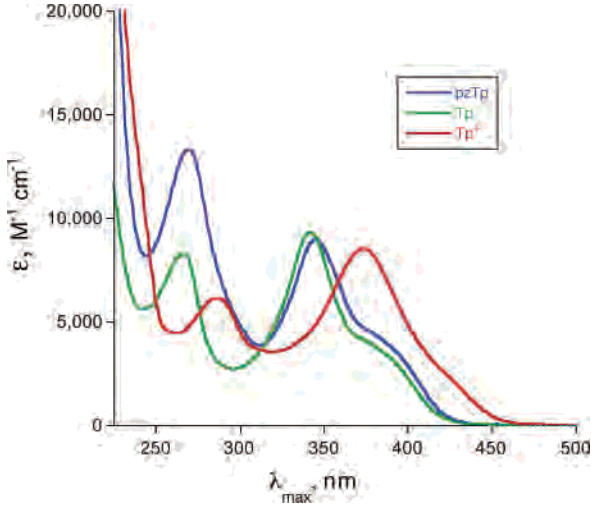

Figure 2. Electronic spectra of $Mn(pzb)_2^+$ complexes in CH_3CN.

manner by oxidation of the corresponding $Mn(pzb)_2$ compounds with $NOSbF_6$. The $[Mn(pzb)_2]SbF_6$ products were isolated as yellow crystals and were characterized by elemental analysis, UV−vis spectroscopy, magnetic moment measurements, electrochemistry, and X-ray crystallography.

Complexes **1**−**3** exhibit magnetic moments of 2.95−3.83 μ_B in the solid state. This range of values is consistent with low-spin d^4 character (spin-only value = 2.83 μ_B) accompanied by an orbital contribution. Magnetic moments in solution (Figure 1) are consistent with these results, although solution and solid-phase values differ by 0.2−0.3 μ_B in individual cases. Measurements of $Mn(Tp^*)_2^+$ were extended to 370 K in DMF-d_7 to explore the possible existence of a low-to-high-spin crossover promoted by the presence of 3,5-dimethyl substituents in this complex. Although μ_{eff} increases by ∼5% between 270 and 370 K, higher temperatures were not attainable, and it is not possible to ascertain if such behavior corresponds to the onset of spin crossover. If spin crossover occurs for **3**, its transition temperature is much higher than that of previous examples involving Mn(III).[18,20]

The electronic spectra of **1**−**3** are shown in Figure 2. Prominent absorptions with $\epsilon = 0.6-1.3 \times 10^4$ M^{-1} cm^{-1} are observed at 267−277 and 342−364 nm, and a shoulder with $\epsilon = 0.2-0.6 \times 10^4$ M^{-1} cm^{-1} is observed at 380−420 nm. The higher-energy bands are likely of charge transfer origin; the origin of the low-energy shoulder is uncertain. Although spin-allowed d−d transitions with log ϵ = 3.2−3.5 have been assigned variously at 27 000−31 000 cm^{-1} in $Mn(CN)_6^{3-}$,[15] the location of such bands in low-spin Mn(III) species has not been established conclusively. The three $Mn(pzb)_2^+$ transitions, which are almost identical in energy for **1** and **2**, are red-shifted by 1000−2000 cm^{-1} in **3**. Similar energetic differences are observed in the transitions of other metal−bis(pzb) complexes[14] and indicate a smaller ligand field strength for Tp*. Intensities of the 342−364 nm band and the shoulder are approximately independent of ligand. However, the intensities of the 267−277 nm band exhibit a significant ligand dependence, pzTp > Tp > Tp*, which parallels the increase in the N−Mn−N bite angle (vide infra).

Structures. ORTEP diagrams and numbering schemes of the $Mn(pzb)_2^+$ cations are shown in Figure 3. Selected bond distances and bond angles are collected in Table 2. In complexes **1**, **2**, and **3** the Mn(III) ion is bound in a facial tridentate manner by the three pyrazole N-2 nitrogens of each ligand at mean distances of 1.974(4), 1.984(5) and 1.996(4) Å, respectively. The close conformity of Mn−N distances within each complex indicates the absence of e_g* occupation, which would characterize a high-spin d^4 center. A much greater dispersion in metal−ligand bond distances is apparent in established high-spin Mn(III) complexes. Examples include four short and two long Mn−O distances at mean values of 1.935(3) and 2.111(4) Å in γ-$Mn(acac)_3$[30a] and 1.94(2) and 2.13(3) Å in molecule 1 of $Mn(trop)_3$,[30b] three short Mn−$N_{pyrrole}$ and three long Mn−N_{imine} distances at 2.054(2) and 2.148(2) Å in Mn(taa),[18a] and three pairs of Mn−N distances at 2.08(1), 2.13(1), and 2.18(1) Å in $Mn(sar)^{3+}$.[17] Moreover, the 1.974−1.996 Å range of Mn−N distances in **1**−**3** and 0.72 Å crystal radius of low-spin Mn(III)[31] are consistent with the 0.69 Å crystal radius of low-spin Fe(III) and Fe−N distances of 1.937(3) Å in $[Fe(t\text{-}BuTp)_2]PF_6$,[32] 1.955(4) Å in $[Fe(t\text{-}BuTp^{Me})_2]PF_6$,[32] 1.956(6) Å in $[Fe(Tp)_2]BF_4$,[33] and 1.964(5) Å in $[Fe(Tp^*)_2]PF_6$.[34] Thus, X-ray crystallography confirms the low-spin character of **1**−**3**.

Tridentate coordination of the two pyrazolylborate ligands in **1** and **2** produces N−Mn−N bite angles of slightly less than 90°, which leads to a small trigonal distortion and effective D_{3d} symmetry in these complexes. However, the

(30) (a) Stults, B. R.; Marianelli, R. S.; Day, V. W. *Inorg. Chem.* **1979**, *18*, 1853−1858. (b) Avdeef, A.; Costamagna, J. A.; Fackler, J. P., Jr. *Inorg. Chem.* **1974**, *13*, 1854−1863.
(31) Shannon, R. D. *Acta Crystallogr.* **1976.**, *A32*, 751−767.
(32) Graziani, O.; Hamon, P.; Thépot, J.-Y.; Toupet, L.; Szilágyi, P. A.; Molnár, G.; Bousseksou, A.; Tilset, M.; Hamon, J.-R. *Inorg. Chem.* **2006**, *45*, 5661−5674.
(33) Calogero, S.; Gioia Lobbia, G.; Cecchi, P.; Valle, G.; Friedl, J. *Polyhedron* **1994**, *13*, 87−97.
(34) Mason, S. J.; Hill, C. M.; Murphy, V. J.; O'Hare, D.; Watkin, D. J. *J. Organomet. Chem.* **1995**, *485*, 165−171.

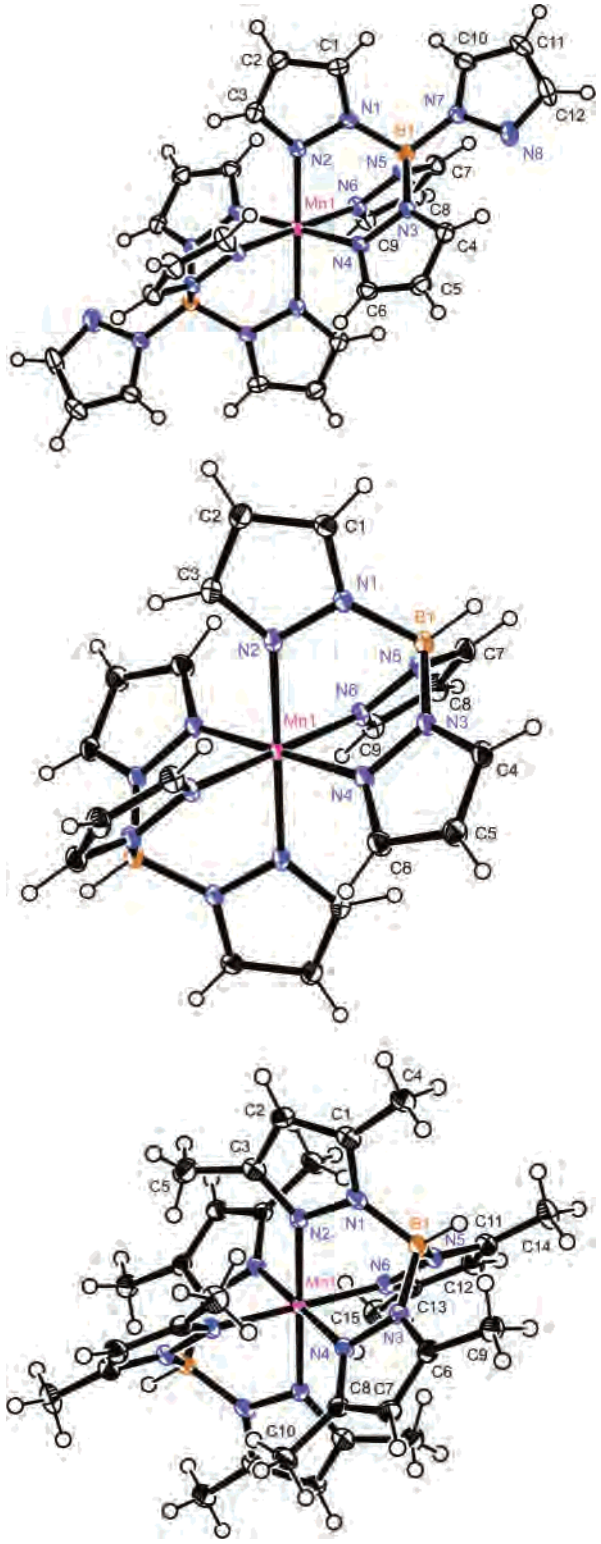

Figure 3. Structures and numbering schemes of the $Mn(pzb)_2^+$ cations of **1**, **2**, and **3** from top to bottom, respectively, with ellipsoids shown at 50% probability.

bite angles increase to 90.0(4)° in **3**, producing an almost perfectly octahedral disposition of N donors in $Mn(Tp^*)_2^+$. In all three complexes, the Mn−N−N−C and Mn−N−N−B torsion angles are close to 180° and 0°, respectively, indicating little titling or twisting of the planar pyrazole rings, and there is little trigonal twisting of the N···N···N faces away from an octahedral arrangement [$\phi = 60(1)°$].

Table 2. Selected Bond Distances (Å) and Bond Angles (deg) for **1**, **2**, and **3**

	1	**2**	**3**
	Distances		
Mn−N2	1.970(2)	1.983(1)	1.998(1)
Mn−N4	1.978(2)	1.979(1)	1.999(2)
Mn−N6	1.974(2)	1.989(1)	1.992(2)
	Angles		
N2−Mn−N4	88.00(8)	87.41(4)	89.82(10)
N2−Mn−N6	87.09(7)	87.78(4)	89.74(10)
N4−Mn−N6	88.65(8)	88.73(4)	90.51(10)
N2−Mn−N4′	92.00(8)	92.59(4)	90.18(10)
N2−Mn−N6′	92.91(7)	92.22(4)	90.26(10)
N4−Mn−N6′	91.35(8)	91.27(4)	89.49(10)
Mn−N2−N1−C1	178.1(2)	177.6(1)	179.4(2)
Mn−N4−N3−C4(C6)[a]	177.0(2)	176.4(1)	178.2(2)
Mn−N6−N5−C7(C11)[b]	176.6(2)	179.5(1)	176.5(2)
Mn−N2−N1−B1	2.5(5)	0.7(1)	1.8(3)
Mn−N4−N3−B1	0.9(2)	2.5(1)	1.1(3)
Mn−N6−N5−B1	4.9(2)	1.4(1)	2.7(3)

[a] C6 in **3**. [b] C11 in **3**.

The crystallographic results for **1**−**3** in conjunction with structures of the corresponding Mn(II)[10,11] and Mn(IV)[12] species allows the combined influence of oxidation state and ligand substitution pattern on the structure of $Mn(pzb)_2^{n+}$ (n = 0, 1, 2) complexes to be examined. These data are compiled in Table 3. The Mn−N distance is the structural parameter most significantly influenced by oxidation state. This distance decreases by 0.26−0.27 Å upon oxidation from Mn(II) to Mn(III), consistent with the conversion of a high-spin $t_{2g}^3e_g^2$ to low-spin t_{2g}^4 configuration. The Mn−N distance decreases further by only 0.02−0.03 Å upon oxidation to t_{2g}^3 Mn(IV). The Mn−N distance also decreases as Tp* > Tp > pzTp in each oxidation state; however, the largest range of such values is 0.034 Å. Bulky 3-position substituents are known to create unfavorable steric interactions in pzb^- complexes, and the mean 3.8, 3.7, and 3.7 Å interligand separations between 3-methyl groups in $Mn(Tp^*)_2$, $Mn(Tp^*)_2^+$, and $Mn(Tp^*)_2^{2+}$, respectively, are consistent with such congestion. However, presence of these groups does not prevent formation of homoleptic bis(Tp*) complexes containing small metal ions such as low-spin Mn^{3+}, low-spin Fe^{3+},[32,34] and Mn^{4+}.[12]

Additional structural differences resulting from changes in ligand or oxidation state are apparent in Table 3. For example, the N···N bite distance increases systematically as pzTp < Tp < Tp* and as Mn(IV) < Mn(III) < Mn(II). However, the N−Mn−N bite angle, which also increases as pzTp < Tp < Tp*, *decreases* as Mn(IV) > Mn(III) > Mn(II). A general expectation[10,35] is that the N···N bite distance will increase and the N−M−N bite angle will decrease as the size of the metal ion increases. The first relationship is illustrated by the lower plot in Figure 4, where the N···N distance is plotted against the M−N bond distance for a series of homoleptic bis(pzb) complexes containing a variety of metal ions and oxidation states, but having a single spin state [low-spin for M(III) and M(IV), high-spin for M(II)]. A

(35) (a) Reger, D. L.; Collins, J. E.; Layland, R.; Adams, R. D. *Inorg. Chem.* **1996**, *35*, 1372−1376. (b) Reger, D. L.; Collins, J. E.; Myers, S. M.; Rheingold, A. L.; Liable-Sands, L. M. *Inorg. Chem.* **1996**, *35*, 4904−4909.

Table 3. Average Distances (Å) and Angles (deg) in Mn−Pyrazolylborate Complexes as a Function of Ligand and Oxidation State

	Mn−N	$(N\cdots N)_{bite}$	Mn···B	$(N-Mn-N)_{bite}$	$(N-Mn-N)_{inter}$	N−B−N	Mn−N−N	Mn−N−C	N_B-N_M-C	Mn−N−N−C	Mn−N−N−B
						Mn(II)					
pzTp[a]	2.236(38)	2.95(4)	3.31(1)	82.7(25)	97.3(25)	109.1(26)	119.8(26)	119.2(21)	132.5(23)	106.1(3)	167.7(87)	11.2(68)
Tp[a]	2.251(32)	2.99(4)	3.29(1)	83.4(21)	96.6(26)	109.3(9)	121.4(7)	117.8(12)	135.9(13)	106.2(7)	178.3(13)	3.6(17)
Tp*[b]	2.270(2)	3.05(1)	3.26(1)	84.5(8)	95.5(10)	109.7(1)	120.8(1)	115.0(1)	135.8(1)	106.2(1)	162.9(1)	19.1(9)
						Mn(III)					
pzTp[c]	1.974(4)	2.74(2)	3.12(1)	87.9(8)	92.1(8)	107.0(3)	117.7(16)	120.8(13)	132.2(14)	106.8(2)	177.2(8)	2.8(20)
Tp[c]	1.984(5)	2.75(2)	3.12(1)	88.0(7)	92.0(7)	106.7(2)	118.8(4)	119.9(3)	133.1(4)	107.0(2)	177.8(11)	1.5(0)
Tp*[c]	1.996(4)	2.82(1)	3.07(1)	90.0(4)	90.0(4)	108.0(1)	118.8(1)	117.2(2)	135.9(2)	106.8(2)	178.0(15)	1.9(8)
						Mn(IV)					
pzTp[d]											
Tp[e]	1.955(6)	2.73(1)	3.11(1)	88.7(3)	91.3(3)	106.0(6)	119.2(6)	119.7(4)	132.3(3)	107.1(1)	175.8(23)	2.5(18)
Tp*[e]	1.972(6)	2.80(1)	3.07(1)	90.3(4)	89.7(4)	107.2(7)	119.2(2)	117.4(2)	135.1(5)	107.5(4)	177.0(24)	3.2(20)

[a] Reference 10. [b] Reference 11. [c] This Work. [d] Structure not available. [e] Reference 12.

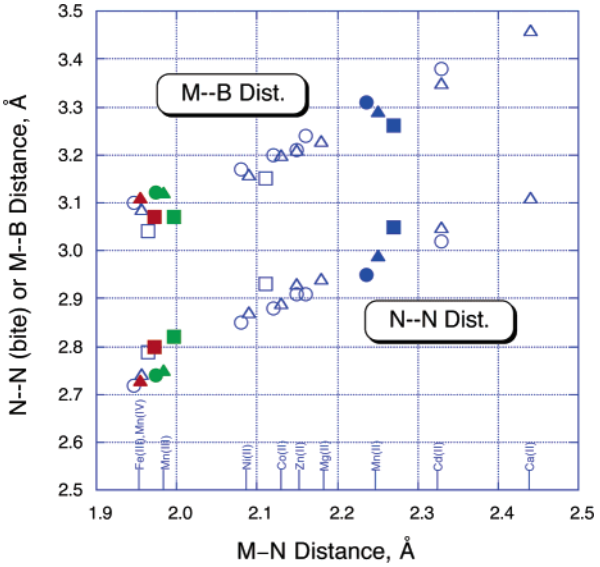

Figure 4. M···B and N···N (bite) distances plotted as a function of the mean M−N distance in metal−bis(pzb) complexes according to *ligand*: pzTp (circles), Tp (triangles), Tp* (squares); *oxidation state*: II (blue), III (green), IV (red); and *metal*: Mn (filled symbols), other metals (open symbols). Sources of structural data are: $Mn(Tp)_2^{2+}$, $Mn(Tp^*)_2^{2+}$, ref 12; $Mn(pzTp)_2^+$, $Mn(Tp)_2^+$, $Mn(Tp^*)_2^+$, this work; $Fe(pzTp)_2^+$, ref 36; $Fe(Tp)_2^+$, ref 33; $Fe(Tp^*)_2^+$, ref 34; $Mn(pzTp)_2$, $Mn(Tp)_2$, ref 10; $Mn(Tp^*)_2$, ref 11; $Ni(pzTp)_2$, ref 10; $Ni(Tp)_2$, ref 37; $Ni(Tp^*)_2$, ref 38 (data are for the Tp^{Me} complex); $Co(pzTp)_2$, ref 10; $Co(Tp)_2$, ref 39; $Zn(pzTp)_2$, ref 10; $Zn(Tp)_2$, ref 40; $Mg(pzTp)_2$, $Mg(Tp)_2$, ref 41; $Cd(pzTp)_2$, ref 42; $Cd(Tp)_2$, ref 43; $Ca(Tp)_2$, ref 41.

correlation is observed between the N···N and M−N distances independent of metal ion and oxidation state. Furthermore, the N···N distance increases as pzTp < Tp < Tp* in parallel with the increase in M−N distance. However, although Table 3 reveals that the N−Mn−N bite angle decreases as the Mn−N distance increases, *this correlation is true only if the identity of the ligand is not changed*.

It also is expected that the distance from the metal to each pzb^- ligand (defined as the length of the M···B vector) will increase as the M−N distance increases. This behavior is confirmed by the trend of the upper plot in Figure 4. However, as the ligand changes from pzTp to Tp to Tp* within a single family of $M(pzb)_2^{n+}$ complexes, there is a systematic *decrease* in the M···B distance and a systematic *increase* in the N−M−N bite angle (Table 3) with increasing M−N bond distance. The contrasting behavior of the M···B and N···N distances as a function of M−N distance in $Mn(pzb)_2^{n+}$ complexes is illustrated by the filled symbols in Figure 4. Such behavior also is found for complete families of $Fe(pzb)_2^+$ and $Ni(pzb)_2$ complexes, which are among the data represented by open symbols in Figure 4.

It has been customary to describe structural deformations within metal−(pyrazolyl)borate complexes in terms of ligand-based changes. Such pzb^- flexibility has been depicted as an opening of the ligand mouth[44] or as a change in the

(36) Trofimenko, S.; Golen, J. A.; Rheingold, A. L.; Yap, G. P. A. Private communication, Cambridge Crystallographic Data Centre, 2004.
(37) Bandoli, G.; Clemente, D. A.; Paolucci, G.; Doretti, L. *Cryst. Struct. Commun.* **1979**, *8*, 965−970.
(38) Cecchi, P.; Gioia Lobbia, G.; Marchetti, F.; Valle, G.; Calogero, S. *Polyhedron* **1994**, *13*, 2173−2178.

Scheme 2

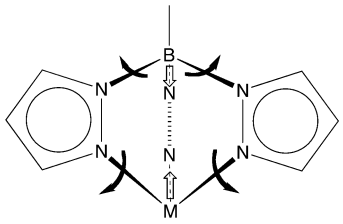

extent of pyramidalization of the boron atom.[45] However, inspection of the data in Table 3 indicates that large changes in structure occur also at the point of metal−ligand contact, where bonds are relatively weak. Thus, in addition to a 0.01−0.03 Å increase in the Mn−N distance, Mn−N−N angles contract by 2.4−4.2° and Mn−N−C angles widen by similar amounts as pzb$^-$ changes from pzTp to Tp to Tp*. Concomitantly, there are small increases of 0.6−1.0° in the N−B−N and N−N−B angles.[46] Thus, there are two components to the structural distortions that arise from the presence of methyl groups at the pyrazole 3-positions. One is contraction of the B−Ct_{N1} distance (Ct_{N1} is the centroid of the plane defined by the pyrazole N-1 nitrogens) upon opening of the N−B−N and N−N−B angles. The other is contraction of the Mn−Ct_{N2} distance (Ct_{N2} is the centroid of the plane defined by the pyrazole N-2 nitrogens) by a hinging or sliding motion of the pyrazole ring at the Mn−N2 juncture. These structural changes are illustrated in Scheme 2. Examination of structural data for Mn(pzb)$_2^{n+}$ complexes reveals that the B−Ct_{N1} and Mn−Ct_{N2} contractions contribute approximately equally to the decrease in Mn···B distance upon passing from pzTp to Tp*.

The above observations provide further insight to the influence of (pyrazolyl)borate substitutents on the properties of their transition metal complexes. Generally, there is a systematic decrease in ligand field strength and an increased tendency for low-to-high-spin crossover in Tp* versus Tp or pzTp complexes.[47] This trend is apparent in the spectroscopic and magnetic properties in Figures 1 and 2. Such changes are thought to arise primarily from the influence of a sterically imposed increase in Mn−N bond distance. However, Mn−N distances increase by only 0.01−0.03 Å upon substitution of Tp* for Tp or pzTp (Table 3); thus, we suggest that changes in the Mn−N−N angles (Scheme 2) also make an important contribution to differences in spectroscopic and magnetic behavior. Because the pyrazole rings are inflexible, their displacement will direct the N2 lone pair orbitals away from the metal leading to less effective overlap and lower ligand field strength. Such distortions, in combination with other factors, are consistent with the proclivity of Tp* and other 3-methyl substituted pzb$^-$ ligands to favor high- versus low-spin states in their metal complexes.

Table 4. Electrochemical Data for Reduction and Oxidation of Mn(pzb)$_2^+$ Complexes[a]

ligand	redox step	$E^{\circ\prime}$ V vs $Fc^{+/0}$	$i_p/\nu^{1/2}AC$ $\mu A\ s^{1/2}\ V^{-1/2}\ cm^{-2}\ mM^{-1}$	$k_{s,h}$ cm s^{-1}
pzTp	III/II	+0.13(1)	500(10)	$7.8(17) \times 10^{-4}$
Tp	III/II	+0.14(1)	630(10)	$1.8(2) \times 10^{-4}$
Tp*	III/II	−0.01(1)	460(40)	$2.6(2) \times 10^{-3}$
pzTp	III/IV	+1.30(1)	750(60)	$1.2(4) \times 10^{-2}$
Tp	III/IV	+1.22(1)	860(30)	$2.1(9) \times 10^{-2}$
Tp*	III/IV	+0.96(1)	580(100)	$1.4(6) \times 10^{-2}$ [b]

[a] Obtained from background-subtracted, resistance-compensated cyclic voltammograms at a glassy carbon dlectrode in 0.1 M $TBAPF_6/CH_3CN$ for $\nu = 0.025-0.25$ V s^{-1}. [b] Background subtraction not applied.

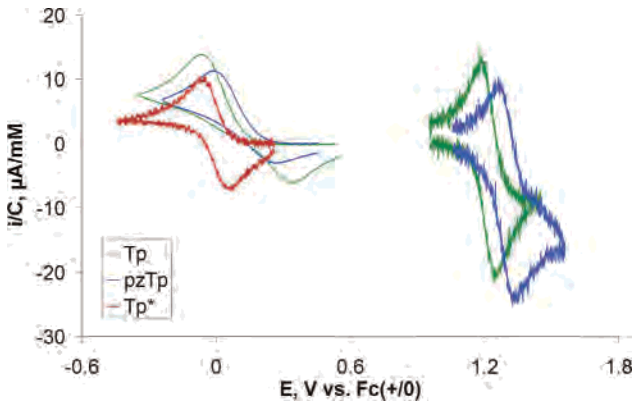

Figure 5. Concentration-normalized cyclic voltammograms for the reduction and oxidation of 1.00 mM **1**, 0.99 mM **2,** and 0.095 mM **3** in 0.1 M $TBAPF_6/CH_3CN$ at $\nu = 0.1$ V s^{-1}. Oxidizing voltammogram of **3** omitted due to large noise content.

Electrochemistry. The electrochemical behavior of complexes **1**−**3** was examined in CH_3CN containing 0.1 M $TBAPF_6$. This work was undertaken to study the Mn(III) → Mn(II) reductions and Mn(III) → Mn(IV) oxidations as primary electrode processes and to acquire more accurate kinetic and thermodynamic data via compensation of solution resistance. Electrochemical data are summarized in Table 4.

The cyclic voltammetric traces in Figure 5 illustrate the chemically reversible reductions and oxidations of Mn(pzb)$_2^+$ complexes, which occur at potentials separated by 1.0−1.2 V. This large spacing is consistent with the metal-based character of the electrode reactions. The $E^{\circ\prime}$ values for each redox step become more positive in the sequence Tp* < Tp < pzTp and encompass a range of 0.1−0.3 V. Such observations are consistent with the results of previous

(39) Churchill, M. R.; Gold, K.; Maw, C. E., Jr. *Inorg. Chem.* **1970**, *9*, 1597−1604.
(40) Nakata, K.; Kawabata, S.; Ichikawa, K. *Acta Crystallogr.* **1995**, *C51*, 1092−1094.
(41) Sohrin, Y.; Kokusen, H.; Kihara, S.; Matsui, M.; Kushi, Y.; Shiro, M. *J. Am. Chem. Soc.* **1993**, *115*, 4128−4136.
(42) Reger, D. L.; Mason, S. S.; Rheingold, A. L.; Ostrander, R. L. *Inorg. Chem.* **1993**, *32*, 5216−5222.
(43) Reger, D. L.; Myers, S. M.; Mason, S. S.; Darensbourg, D. J.; Holtcamp, M. W.; Reibenspies, J. H.; Lipton, A. S.; Ellis, P. D. *J. Am. Chem. Soc.* **1995**, *117*, 10998−11005.
(44) De Bari, H.; Zimmer, M. *Inorg. Chem.* **2004**, *43*, 3344−3348.
(45) Reger, D. L.; Gardinier, J. R.; Elgin, J. D.; Smith, M. D.; Hautot, D.; Long, G. J.; Grandjean, F. *Inorg. Chem.* **2006**, *45*, 8862−8875.
(46) Similar structural differences about B and the bonding pyrazole N's are apparent in the recently reported crystal structures of Fe(*t*-BuTp)$_2$PF$_6$ and Fe(*t*-BuTp^{Me})$_2$PF$_6$.[32] Here, Fe−N−N angles contract from 122.2(4)° in Fe(*t*-BuTp)$_2$PF$_6$ to 118.4(1)° in Fe(*t*-BuTp^{Me})$_2$PF$_6$, while smaller changes of 0.5−1.5° occur in the N−B−N and N−N−B angles. N−Fe−N bite angles increase from 87.8(5)° in Fe(*t*-BuTp)$_2$PF$_6$ to 90.1(2)° in Fe(*t*-BuTp^{Me})$_2$PF$_6$. Similar comparative differences occur in the structures of [Fe(Tp)$_2$]BF$_4$[33] and [Fe(Tp*)$_2$]PF$_6$[34] and Ni(Tp)$_2$[10] and Ni(Tp^{Me})$_2$.[38]
(47) Long, G.J.; Grandjean, F.; Reger, D.L. In *Spin Crossover in Transition Metal Compounds I*; Gütlich, P., Goodwin, H.A., Eds.; Springer: Berlin, 2004; pp 91−122.

electrochemical studies of metal−bis(pzb) complexes.[14,48] The $Mn(pzb)_2^+$ oxidations exhibit voltammetric peak current parameters, $i_p/v^{1/2}AC$, that are consistent with a one-electron transfer involving reactants of this size in CH_3CN.[49] The $Mn(pzb)_2^+$ reductions also exhibit $i_p/v^{1/2}AC$ parameters that are consistent with one-electron stoichiometry, but values are smaller because of the slow kinetics of Mn(III)/Mn(II) electron transfer.

The difference in kinetics of the two-electrode reactions is apparent from the peak potential separations in Figure 5. The $Mn(pzb)_2^+$ oxidations are nearly nernstian and yield $k_{s,h}$ values of 0.01−0.02 cm s^{-1} with little ligand dependence. The $Mn(pzb)_2^+$ reductions are 1−2 orders of magnitude slower and exhibit $k_{s,h}$ values of 7.8×10^{-4}−2.6×10^{-3} cm s^{-1} with significant ligand dependence (Table 4). These findings are consistent with results reported earlier in 1,2-dichloroethane,[14] where individual $k_{s,h}$ values are 2−4 times smaller than those reported here.

The electrode kinetic data in conjunction with structural and magnetic results (vide supra) indicate that Mn(II) → Mn(III) → Mn(IV) oxidation of $Mn(pzb)_2^{n+}$ complexes proceeds through a low-spin Mn(III) rather than high-spin Mn(III) oxidation state (Scheme 1). Thus, each Mn(III)/Mn(II) electrode reaction is accompanied by a change in metal atom spin state:

$$\text{low-spin } Mn(pzb)_2^+ + e^- \leftrightarrows \text{high-spin } Mn(pzb)_2 \quad (1)$$

Mn(III)/Mn(II) electron-transfer reactions frequently are slow.[50] Although underlying causes are not well established in most instances, the structural and magnetic information reported here confirms that spin crossover occurs and is a distinguishing feature in the kinetics of $Mn(pzb)_2^{+/0}$ versus $Mn(pzb)_2^{2+/+}$ electrode reactions.

Knowledge of the general path of Mn(II) → Mn(III) → Mn(IV) oxidation, however, does not reveal the mechanistic details of reaction 1. Electron transfer accompanied by spin crossover[13] may proceed through a low-spin Mn(II) or high-spin Mn(III) intermediate via coupled electron transfer and spin-change steps or in a concerted manner from t_{2g}^4 Mn(III) to $t_{2g}^3e_g^2$ Mn(II). In either case, large thermodynamic or kinetic barriers must be overcome, resulting in slow transfer. The ligand dependence of Mn(III)/Mn(II) electron-transfer rates is of interest with regard to this mechanistic puzzle. As shown in Table 4, $k_{s,h}$ decreases as Tp* > pzTp > Tp for reaction 1. This is the *inverse* of the sequence found for comparable $Fe(pzb)_2^{+/0}$ [13b] and $Co(pzb)_2^{+/0}$ [14] couples, which also involve reduction of a low-spin M^{3+} to high-spin M^{2+} center. Further investigation is needed to understand this difference and the fundamental relationships between structure and electron-transfer rate for these reactions. However, we note that the Tp* > pzTp > Tp sequence of Mn(III)/Mn(II) rates (Table 4) parallels the apparent high-spin content of $Mn(pzb)_2^+$ complexes (Figure 1). This suggests a greater component of reaction via a high-spin intermediate pathway for $Mn(pzb)_2^{+/0}$ reactions versus those of $Fe(pzb)_2^{+/0}$ and $Co(pzb)_2^{+/0}$.

Summary and Conclusions

Three manganese(III)−bis[poly(pyrazolyl)borate] complexes have been prepared by $NOSbF_6$ oxidation of the corresponding Mn(II) compounds and characterized by X-ray crystallography and electrochemical, spectroscopic, and magnetic methods. These homoleptic $Mn(pzb)_2^+$ species are uncommon examples of low-spin Mn(III). Presence of methyl groups at the 3-position of the pyrazole rings does not prevent formation of low-spin $Mn(Tp^*)_2^+$ and does not incur crossover to its high-spin form under ambient conditions. Examination of structural data from 23 metal−bis(pzb) complexes reveals that significant adjustments in M−N−N and M−N−C, as well as in N−B−N and N−N−B, angles occur in the presence of 3-methyl substituents. These structural changes appear to be equally or more important than simple metal−ligand bond lengthening in accommodating the steric demands of 3-methyl groups in bis(Tp*) complexes.

$Mn(pzb)_2^+$ complexes undergo electrochemical reduction and oxidation to $Mn(pzb)_2$ and $Mn(pzb)_2^{2+}$. The Mn(III)/Mn(II) electrode reactions are accompanied by a change in metal-atom spin state ($t_{2g}^4 \rightarrow t_{2g}^3e_g^2$) and exhibit electrochemical electron-transfer rate constants 1−2 orders of magnitude smaller than those of the corresponding Mn(III)/Mn(IV) ($t_{2g}^4 \rightarrow t_{2g}^3$) oxidations. The rate constants for Mn(III)/Mn(II) reduction decrease as Tp* > pzTp > Tp, which is the inverse of the sequence found for comparable $Fe(pzb)_2^{+/0}$ and $Co(pzb)_2^{+/0}$ reactions.

Acknowledgment. M.-H.B. thanks the National Institutes of Health (HG-003894), the Research Corporation (Cottrell Scholar Award), and the National Science Foundation (0116050 to Indiana University) for financial support. R.L.L. acknowledges the Department of Education for a GAANN Fellowship. F.A.S. acknowledges the National Science Foundation (CHE-9988694) for financial support. The authors wish to thank Dr. Maren Pink for the structural determinations.

Supporting Information Available: Crystallographic data for compounds **1**−**3** in CIF format and electrode kinetic data as a function of sweep rate. This material is available free of charge via the Internet at http://pubs.acs.org.

IC062224+

(48) Onishi, M.; Kumagae, S.; Asai, K.; Kawano, H.; Shigemitsu, Y. *Chem. Lett.* **2001**, 96−97.
(49) Bradbury, J. R.; Schultz, F. A. *Inorg. Chem.* **1986**, *25*, 4408−4416.
(50) Instances of slow Mn(III)/Mn(II) electron transfer include electrochemical: (a) $Mn(NH_3)_6^{3+/2+}$, $k_{s,h} = 6.5 \times 10^{-5}$ cm s^{-1}; Brown, O. R.; Clarke, S. *J. Electroanal. Chem.* **1976**, *70*, 87−93; (b) $Mn(tripod)_2^{+/0}$, $k_{s,h} = 7 \times 10^{-7}$ cm s^{-1}; Kölle, U.; Engler, U. *Eur. J. Inorg. Chem.* **2002**, 165−170.; and homogenous examples: (c) $Mn(H_2O)_6^{3+/2+}$, $k_{ex} = 1 \times 10^{-4}$ M^{-1} s^{-1}; Macartney, D. H.; Sutin, N. *Inorg. Chem.* **1985**, *24*, 3403−3409. (d) $[Mn(edta)(H_2O)]^{-/2-}$, $k_{ex} = 7 \times 10^{-1}$ M^{-1} s^{-1}; Macartney, D. H.; Thompson, D. W. *Inorg. Chem.* **1989**, *28*, 2195−2199.